Journal of Power Sources 242 (2013) 520–526

Contents lists available at SciVerse ScienceDirect

Journal of Power Sources

journal homepage: www.elsevier.com/locate/jpowsour

Combined production and purification of hydrogen from methanol using steam iron process in fixed bed reactor

R. Campo, P. Durán, J. Plou, J. Herguido, J.A. Peña*

Catalysis, Molecular Separations and Reactor Engineering Group (CREG), Aragón Institute of Engineering Research (I3A), Universidad Zaragoza, Mariano Esquillor s/n, Ed. I+D, 50018 Zaragoza, Spain

HIGHLIGHTS

- Production and purification of hydrogen departing from methanol by steam–iron.
- Methanol as featured compound of alcoholic fraction of bio-oil for reductions.
- Doped iron oxide as reactive material.
- Steam as oxidative agent to generate purified hydrogen.
- Highly structured carbon deposits act as inert during oxidation stages.

GRAPHICAL ABSTRACT

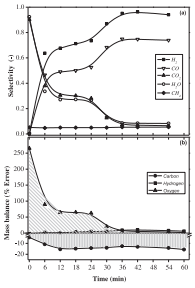

ARTICLE INFO

Article history:
Received 23 January 2013
Received in revised form
8 May 2013
Accepted 27 May 2013
Available online 5 June 2013

Keywords:
Bio-oil
Hydrogen
Production
Methanol
Steam–iron
Redox

ABSTRACT

A research work is being conducted to study the combined production and purification of hydrogen by means of redox processes departing from biomass fast pyrolysis oils (bio-oils). To achieve that goal, methanol has been used as featured material because it is the most representative compound of the alcoholic fraction of bio-oils. The study has been carried out in a fixed bed reactor where methanol decomposes in H_2 and CO when gets in contact with a reactive solid based in an iron oxide at temperatures above 600 °C. During the first stage of the "*steam–iron*" process, reactive gases reduce the iron oxide to metallic iron. Afterward, in a following step, the previously reduced iron is reoxidized by steam producing a high purity hydrogen stream. Although coke deposition does exist during the reducing stage, this behaves as inert during the reoxidation process. Coke inert role has been corroborated by GC, SEM and TEM techniques, showing that carbon deposits were constituted by ordered structures (carbon nanotubes). The determination of the hydrogen production along successive cycles allowed the evaluation of the effect of temperature and alternating reactive atmospheres on the stability of the solid, as well as the optimum conditions for such purpose.

1. Introduction

Nowadays, there exists a growing need for developing renewable energy sources apart from the traditional fossil fuels. In this context, fuels obtained from the pyrolysis of biomass (e.g., forest, crop and industrial wastes) represent an interesting choice due to the renewability and low cost of these raw materials. Bio-oil is the liquid phase generated in the biomass fast pyrolysis. It is a complex mixture of oxygenated organic compounds with a very different composition from that of petroleum derived fuels. The mixture can be very different according to biomass feedstock or pyrolytic process conditions used [1]. Its constituents are normally grouped in four main fractions, classified by its chemical functional groups and its solubility in water and diethyl ether. They are often labeled as alcoholic, acidic, aldehydic and phenolic fractions. In particular, the

* Corresponding author. Tel.: +34 976 762390; fax: +34 976762043.
E-mail address: jap@unizar.es (J.A. Peña).

0378-7753/$ – see front matter © 2013 Elsevier B.V. All rights reserved.
http://dx.doi.org/10.1016/j.jpowsour.2013.05.146

bio-oil alcoholic fraction might be present in percentages close to 10% (w), being methanol the major compound within this phase [2]. Bio-oil shows a high reductive potential, but its characteristics strongly depend on its composition. Several authors have devoted efforts in the near past to determine the feasibility of using bio-oils as renewable sources in hydrogen production by means of redox processes, and specifically by the *steam–iron process* (SIP) [3–5]. All these meritorious works were performed using bio-oils derived from different feedstock, not taking into account the variations in behavior that could arise from the differences in composition depending on the source and thermal treatment. In this context, an attempt to systematically study the redox power of the different fractions of the bio-oil is being carried out in our laboratory. Accordingly, methanol has been chosen as a model compound for representing the alcoholic fraction of bio-oil.

At temperatures above 500 °C, methanol is unstable and decomposes to formaldehyde, syngas (CO and H_2), or filamentous carbon, hydrogen and steam [6]. The decomposition of methanol according to these reactions (r.1)–(r.3) results in a product gas stream with reducing properties.

$$CH_3OH \rightleftharpoons CH_2O + H_2 \quad \text{(r.1)}$$

$$CH_3OH \rightleftharpoons 2H_2 + CO \quad \text{(r.2)}$$

$$CH_3OH \rightleftharpoons H_2 + H_2O + C_{(s)} \quad \text{(r.3)}$$

Due to these gas stream characteristics, it might be used as a reducer feed in the *Steam Iron Process* (SIP) [7]. SIP is one of the oldest methods for producing purified hydrogen departing from the exhaust gases of coal gasification processes. This gas reacts with iron oxides to produce a reduced form of the solid. The reduced iron oxide is later on re-oxidized with steam to form magnetite and hydrogen.

The SIP usage proposed in this work has two consecutive steps. In the first one (reduction), both H_2 and CO (and eventually formaldehyde) from the methanol decomposition will reduce a hematite bed to metallic iron. In this way, CO_2 and water will be obtained as major gaseous products. In a subsequent step (oxidation), metallic iron will be oxidized using steam to generate hydrogen [8].

The first step, comprising iron oxides reduction to metallic iron, is mediated by the presence of H_2 and CO. Reduction of hematite to magnetite can be described by reactions (r.4) and (r.5):

$$3Fe_2O_3 + H_2 \rightleftharpoons H_2O + 2Fe_3O_4 \quad \text{(r.4)}$$

$$3Fe_2O_3 + CO \rightleftharpoons CO_2 + 2Fe_3O_4 \quad \text{(r.5)}$$

Accordingly, (r.6)–(r.9) describe the reduction of magnetite to metallic iron:

$$Fe_3O_4 + H_2 \rightleftharpoons H_2O + 3FeO \quad \text{(r.6)}$$

$$Fe_3O_4 + CO \rightleftharpoons CO_2 + 3FeO \quad \text{(r.7)}$$

$$FeO + H_2 \rightleftharpoons H_2O + Fe \quad \text{(r.8)}$$

$$FeO + CO \rightleftharpoons CO_2 + Fe \quad \text{(r.9)}$$

Others reactions such as methanation (r.10), water gas shift reaction (r.11) or reverse *Boudouard* reaction (r.12) could take place as well:

$$3H_2 + CO \rightleftharpoons H_2O + CH_4 \quad \text{(r.10)}$$

$$H_2O + CO \rightleftharpoons H_2 + CO_2 \quad \text{(r.11)}$$

$$2CO \rightleftharpoons CO_2 + C_{(s)} \quad \text{(r.12)}$$

In the subsequent oxidation step, steam is fed to the solids bed resulting from the previous reduction stage. Steam oxidizes metallic iron (r.13) accomplishing reactions (r.8) and (r.6) in its reverse direction. Reverse reaction (r.4) is not attained because steam is not able to regenerate iron to hematite due to thermodynamic restrictions at the experimental conditions tested [9].

$$4H_2O + 3Fe \rightleftharpoons Fe_3O_4 + 4H_2 \quad \text{(r.13)}$$

At the same time, carbonaceous deposits in the solid bed might be eventually gasified by the water fed to the reactor (r.14).

$$C_{(s)} + H_2O \rightleftharpoons CO + H_2 \quad \text{(r.14)}$$

In several previous works of our research group, the SIP feasibility has been analyzed using $H_2 + CH_4$ streams coming from natural gas thermal decomposition [10–12] or synthetic biogas ($CH_4 + CO_2$) streams [13–15] as reducing raw materials. Although good results were obtained, a problem arose related to the stability of iron oxides along several reduction + oxidation cycles [16]. The addition of small quantities of Al, Cr and Ce to the iron oxides, greatly improved the stability and oxidation activity of the solids during the repeated reduction–oxidation cycles [17]. Following this pace, an optimum percentage of metal additives was found for which the maximum amount of hydrogen storage density (i.e. mg H_2 released by 100 mg of iron), was kept practically constant along cycles.

In this context, the main objective of this work has been to analyze the feasibility of producing pure hydrogen from a methanol stream, considered as a prominent part of bio-oil composition. To this end, previously optimized solid has been used in a fixed bed reactor configuration, analyzing both its performance for the steam iron process and its stability after several reduction–oxidation cycles, paying special attention to the problem of coke deposition on the solid surface during the reduction step and a possible phenomenon of hydrogen contamination by gaseous carbonaceous species upon reoxidation of the solid.

2. Experimental

The solid used as reactant was a lab made iron oxide (hematite) doped with alumina and ceria, having the following composition as weight percentages: Fe_2O_3 98%; Al_2O_3 1.75%; CeO_2 0.25%. This oxide will be called '*triple oxide*' from now on. The additives were included in order to improve pure hematite redox characteristics [18–20]. Thus, alumina addition decreases sintering effects over the iron oxide, while ceria is used as a promoter in redox reactions where atomic oxygen is involved [21]. This formula was previously tested and validated as optimal for high performance and stability in hydrogen purification using gas mixtures from natural gas pyrolysis and redox processes [22,23].

The oxide was synthetized by a sol–gel method based in the precipitation of citrates [24]. The departing materials were $Fe(NO_3)_3 \cdot 9H_2O$, $Al(NO_3)_3 \cdot 9H_2O$ and $Ce(NO_3)_4 \cdot 6H_2O$, at least 99% purity, all of them from *Sigma–Aldrich*. A metallic nitrate solution (1 M) was heated to 80 °C and then citric acid solution (1 M) was poured into the beaker. After 2 h stirring, the gel was formed. It was later dried at 60 °C for 12 h and calcined in two steps at 350 °C for 2 h and 800 °C for 8 h. The final solid was sieved to a particle diameter of 160–200 μm. Its BET surface was determined to be around 15 $m^2\ g^{-1}$.

The experimental device used for reaction tests consisted of a cylindrical quartz reactor (inner diameter of 13 mm). A fixed bed of solid was introduced inside the reactor with a load of 2.5 g of a

mixture 63.75%w triple oxide and 36.25%w inert oxide (SiO_2). Silica was added to keep a minimum temperature profile along the bed and to diminish preferential pathways of the gas stream in its cross-sectional distribution.

In both reduction and oxidation experiments, the reaction system was operated at room pressure and a 250 N mL min^{-1} total gas flow was fed into the top inlet of the reactor. This flowrate has been proven large enough to avoid external diffusional control. Gas feed composition was different depending on the reaction step being tested: reduction steps consisted of methanol streams (partial pressure of 0.1 bar) diluted in He, while in oxidation steps the feed consisted of steam (partial pressure of 0.25 bar) diluted in He. Argon (partial pressure of 0.05 bar) was used as internal standard in order to facilitate the quantification of products from outgoing gas streams analysis. Flowrates for both methanol and water were dosed as liquid phases, using HPLC pumps *Shimatzu LC20AT*. The liquids were thereafter vaporized and fed to the reactor incoming gas stream. Inert gases (He and Ar) were added using mass flow meters *Brooks 5850*.

The reactor was contained inside an electric oven. Temperature for reduction experiments ranged from 600 to 800 °C according to thermogravimetric measurements performed on the solid with methanol diluted in nitrogen as reductive gas (*Netzsch STA 449F3 JUPITER*). Temperature limits were selected based on the reduction temperature of hematite to metallic iron (weight losses attributed to Fe_2O_3 to Fe_3O_4 transformation – from 340 to 383 °C, and Fe_3O_4 to Fe – 600–720 °C – respectively) and avoiding sintering as far as possible. The oxidation step was always performed at 500 °C according to the previous experience of the subscribing research group [11,16].

The exhaust gases, including steam and eventually remaining methanol were analyzed using a gas chromatograph (TCD) *Agilent 7890A*.

The surface morphology of fresh and used solids was analyzed by field emission scanning electronic microscopy (FESEM), on a *Carl Zeiss Merlin* model operating with 5 kV, and by transmission electron microscopy (TEM) on a *JEOL 2000 FXII* (200kV) unit. XRD diffractograms were performed with a *Rigaku D/Max 2500/PC* using the Cu-Kα radiation ($\lambda = 1.541$ Å) operated at 60 kV and 300 mA. The measurements ranged from 15° to 85°.

3. Results

3.1. Methanol decomposition on triple oxide

Working at the above mentioned conditions, a complete methanol conversion has always been verified during reduction steps regardless of the initial oxidation state of the triple oxide. In order to elucidate the effect of this solid on the decomposition of methanol, two different trials were carried out and compared. On the one hand, blank experiments in which silica was the only solid in the bed, and on the other hand, experiments with triple oxide (plus silica as solid diluent) previously reduced with H_2 up to achieve complete reduction of the iron oxide to metallic iron.

In both cases a stable behavior was observed along time with constant methanol conversion and products distribution. Table 1 shows the values of conversion of methanol and yields toward products achieved at 700 °C and a partial pressure of methanol of 0.1 bar. Methanol decomposition seems to be only thermic when using silica bed; its conversion roughly reaches 9.7% and there is a small generation of H_2O and CH_4 as primary products. Also a minimum quantity of CO was generated. However, it does not exist generation of H_2 and/or CO_2. Apparently, a slight methanol decomposition (r.2) and (r.3) followed by methanation reaction (r.10) takes place. When triple oxide previously reduced is used instead (no lattice oxygen coming from the oxide contributes to the reactions), the decomposition is mainly described by reaction (r.2) producing high yields of hydrogen and carbon monoxide (H_2 yield ~ 95%, CO yield ~ 74.7%), being this an indicator of the catalytic role of the triple oxide. Thus, minimum quantities of H_2O and CH_4 from methanation reaction (r.10) were detected, being results in accordance with the previous ones. Also CO_2 is obtained. It might be produced from WGS reaction and *Boudouard's* disproportionation (r.11) and (r.12). The explanation for this behavior can be found in the fact that iron oxides exert a strong catalytic effect favoring the instantaneous decomposition of methanol, mainly to CO and H_2 [25–27].

Table 1
Comparison of conversion of methanol (%) and yields to different products (%) using a blank bed (SiO_2) and a triple oxide bed. $T = 700$ °C, $p_{CH_3OH} = 0.1$ bar.

	X_{CH_3OH}	Y_{CO}	Y_{H_2}	Y_{CO_2}	Y_{H_2O}	Y_{CH_4}
SiO_2	9.7	0.9	0.0	0.0	6.4	3.6
Triple oxide	100.0	74.7	95.0	7.2	8.3	5.4

Fig. 1 shows an XRD diffractogram depicting the evolution of crystalline species present in the solid along alternated (up to three) reduction–oxidation cycles. Fig. 1a shows the diffractogram of a fresh solid sample prior to any reaction. It exhibits the characteristic peaks of Fe_2O_3. Since Al_2O_3 and CeO_2 are present in a low proportion (1.75 and 0.25%w respectively) their presence is not detected.

3.2. Triple oxide reduction by methanol

In order to describe the distribution of reactants and products along time, a standard reduction experiment was conducted at 700 °C, $p_{CH_3OH} = 0.1$ bar, $Q = 250$ N mL min^{-1}, $W_0 = 2.5$ g. Since methanol was not detected in the exhaust gases of the experiment with triple oxide, it seems reasonable that decomposition reactions (r.1)–(r.3) totally displace reactants to H_2 and CO formation.

Fig. 2a shows the selectivity toward products obtained for fresh triple oxide reduction at 700 °C. During the first stage (around 6 min), hematite to magnetite reduction occurs according to reactions (r.4) and (r.5) by means of emerging H_2 and CO provided by catalytic decomposition of methanol. Thus, selectivity to H_2 and CO at the beginning is low because of quick depletion of the reduction stream by the quick reduction of hematite to magnetite. Meanwhile, selectivity to their oxidized products (H_2O and CO_2) achieves

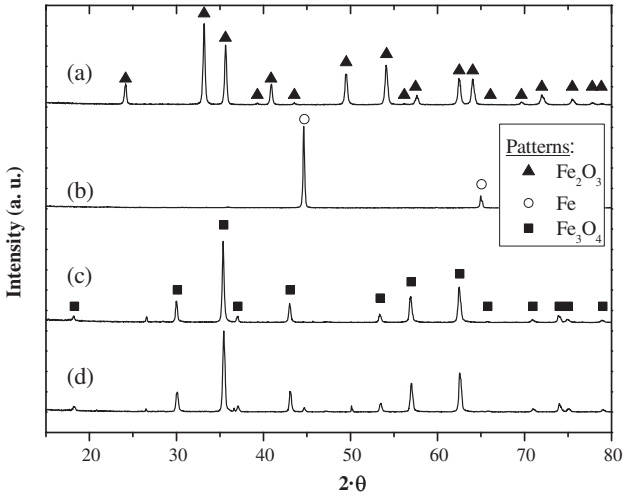

Fig. 1. XRD stacked diffractograms of solid samples after different reduction–oxidation cycles (reduction @700 °C, oxidation @500 °C): (a) fresh solid; (b) after first reduction with methanol; (c) after first reoxidation with steam; (d) after three redox cycles (three times reduced with methanol and reoxidized with steam).

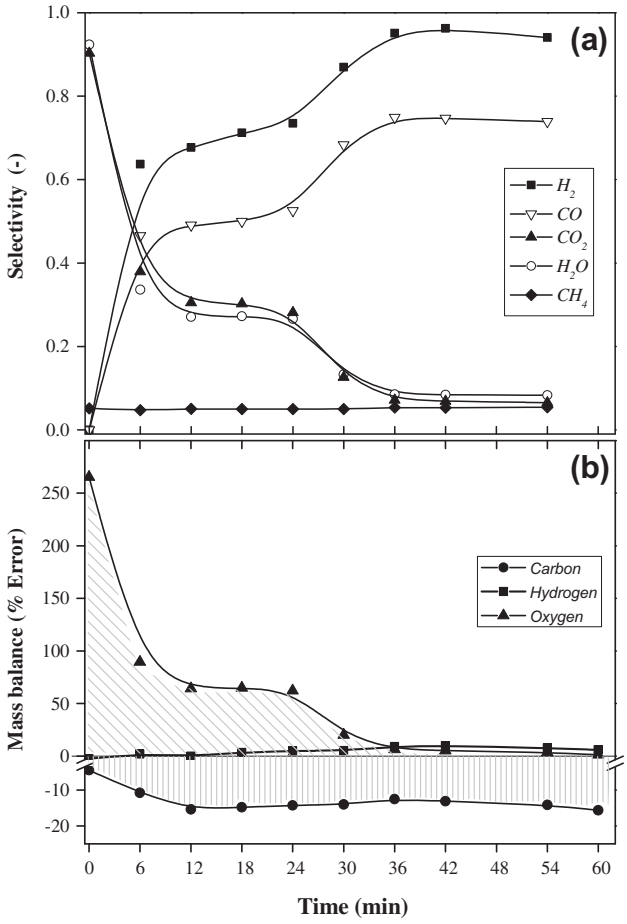

Fig. 2. (a) Temporal evolution of selectivity toward products in the reduction step of fresh triple oxide with methanol. (b) Atomic mass balance closures. $T = 700$ °C.

high values. This behavior indicates the fast reduction rate for this reduction step.

During the second stage, solid reduces from magnetite to metallic iron (up to 24 min) owing to reactions (r.6)–(r.9). Reaction rate is clearly lower than in the previous stage and there is a slight increase in selectivity toward H_2 and CO. The reason for this rate detriment could be the thermodynamic pseudoequilibrium between reductive species (H_2 and CO) and their corresponding oxidized species (H_2O and CO_2). Small amounts of these products present in the reactive atmosphere can slow down the reduction itself [28,29].

The end of solid reduction occurs at around 36 min. From this moment on, the gas selectivity curves show a stable behavior with high values for H_2 and CO and consequently low values (lower than 10%) for oxidized species (H_2O and CO_2) according to reactions (r.2) and (r.3). Regarding to the solid, its lattice oxygen contribution is null since it has been completely reduced. This fact has been corroborated by XRD analysis (see Fig. 1b), where no other peaks different from metallic iron, are present. Therefore from this point, product selectivity is only due to gas interactions and where metallic iron behaves only as catalyst of methanol decomposition. In fact, yields to different gas products remain constant after 36 min (Fig. 2a), and similar to the values previously shown in Table 1.

The deviation in the elemental mass balance for C, H and O is represented in Fig. 2b as the difference between the output and input molar flow streams for these elements, given in a percentile basis. A good balance closure can be observed for hydrogen; however, a very high excess of oxygen is obtained during the first reduction minutes. The curve of oxygen excess matches very well with those of CO_2 and H_2O, as species produced in the reduction of the triple oxide (see Fig. 2a). The oxygen contribution from the solid along the experiment can be calculated from the area under the curve representing the mass balance (i.e., oblique lines filled area in Fig. 2b). The comparison between the obtained value and the theoretical one (i.e., the oxygen content in the triple oxide solid loaded in the bed) agrees very well at all tested temperatures with errors lower than 2% in mass. Regarding carbon curve, a deficit is always perceived. It increases with time-on-stream reaching a nearly constant value around −18% from approximately 12 min on. It can be established that carbon deposition is continuously produced over solid particle surface, causing a decrease in selectivity toward carbonaceous products in exhaust gases.

3.3. Temperature effect over reduction stage

Temperature influence in the solid reduction step was studied by means of experiments performed between 600 and 800 °C. Fig. 3 presents the evolution with the time-on-stream of the water selectivity, which has been selected as variable to analyze the redox solid behavior in this step.

At 800 °C, around 30 min are required to achieve complete solid reduction. At this temperature, generation of carbonaceous material over solid surface was discarded because it was not detected by carbon mass balance closure deficit. Due to the high reduction rate, the restrictions imposed by H_2/H_2O and CO/CO_2 equilibriums (shown by a short plateau from 12 to 18 min), are not as significant as at lower temperatures. Temperature affects inhibition of the reduction reaction because water content in the stream is so high that pseudo-equilibrium between reactants and product is achieved. This fact is particularly visible for experiments at 600 °C for which a plateau zone extends from around 6 min to up to 48 min. At this moment selectivity drops to minimum values according to lower proportions of water in the products stream.

The lower is the reduction temperature the higher is the time to obtain complete reduction of the solid (36 min at 700 °C, 42 min at 650 °C, and more than 60 min at 600 °C). Additionally, as temperature is diminished, coke deposition becomes more appreciable. This has been contrasted by carbon mass balance closure deficit. The lower the temperatures, the higher the deficit in carbon balance: around 30% at 600 °C, 19% at 650 °C, 15% at 700 °C and only around 7.5% for 800 °C.

Therefore, reduction temperature greatly influences how methanol is decomposed. It affects the products distribution, in such a way that low temperatures generate more CH_4, H_2O, CO_2 and $C_{(s)}$.

3.4. Oxidation step with steam

After the reduction step in which the triple oxide is transformed into metallic iron, the next step consists of an oxidation with steam [11], according to reaction (r.13). This oxidation step was always carried out at 500 °C regardless of the temperature used during the previous reduction. In Fig. 4, temporal evolution of steam conversion is shown for fixed beds of solids coming from previous reduction step at different temperatures. As it is shown, reduction step temperature greatly affects solid regeneration degree during the subsequent oxidation step. The initial conversion obtained is slightly higher than 80% for solids with low temperature reductions. Higher conversion is not achieved due to thermodynamic restrictions involved in steam conversion [30]. Fig. 1c and d shows the XRD diffractograms of re-oxidized solid samples after the first cycle and after three consecutive cycles. It seems clear that the crystalline structure corresponds to Fe_3O_4. As with the fresh sample, no peaks attributed to alumina or ceria were detected. No significant differences are perceived between the one cycle (Fig. 1c)

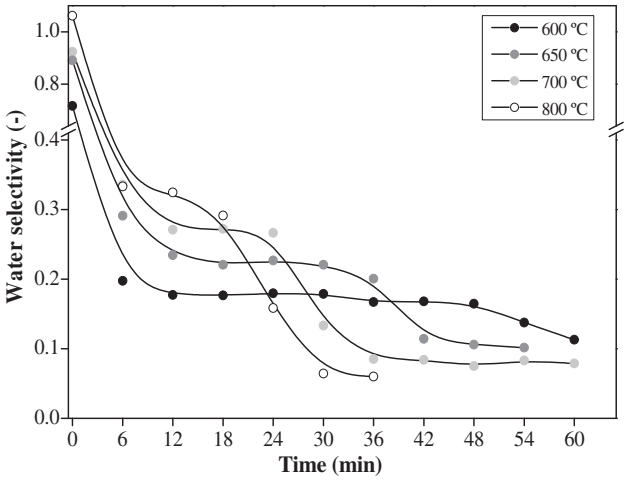

Fig. 3. Temporal evolution of selectivity toward H_2O during the reduction step of fresh triple oxide with methanol: effect of temperature.

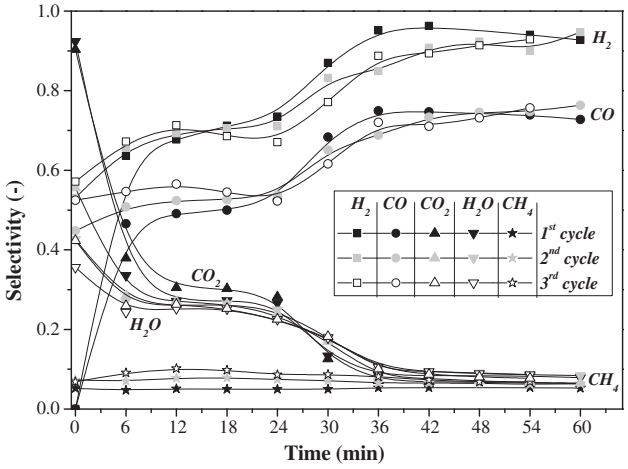

Fig. 5. Temporal evolution of products selectivity in the reduction step of fresh triple oxide with methanol, as a function of the cycle number. $T = 700$ °C.

and three cycles (Fig. 1d) diffractograms, supporting the thesis that although carbon deposition is clearly present, the crystalline structure has not substantially been changed even after three cycles. This is consistent with the distribution of products during the three consecutive reductions shown in Fig. 5.

At higher reduction temperatures (800 °C), water conversion is remarkably lower during the first minutes and its consumption period lasts longer than for solids coming from lower reduction temperatures. This drop in solid activity must be attributed to the thermal sintering supported by the solid during the reduction step. The lower is the reduction temperature, the higher is the kinetics and consequently the lower is the time to obtain complete oxidation of the solid.

It is important to notice that, regardless of the temperature used in previous reduction, coke deposited is not gasified appreciably during the oxidation step in the above mentioned experimental conditions. Neither CO nor CO_2 were detected in exhaust gases by GC. These products should be formed in the gasification with steam of carbonaceous deposits, and they should be detectable by gas chromatography whereof detection limits were measured at 50 ppm for CO and CO_2 in the outlet gas stream. In summary, carbonaceous depositions are behaving as inert, and the obtained hydrogen maintains high purity standards to be used in PEM fuel cells (CO_x concentration < 50 ppm). This can be a good result for the possible practical application of the process, but at that point arises the problem of the possible accumulation of coke in successive redox cycles.

3.5. Successive redox cycles

An experiment consisting of several redox cycles was conducted in order to determine the decay in activity of the iron oxide after each reduction and oxidation step. This behavior might be due to the alteration of the solid structure with alternated atmospheres (methanol and water) [11], thermal sintering and increasing coke deposition.

Fig. 5 shows the selectivity toward products during the reduction step at 700 °C of three successive redox cycles. As it can be seen, selectivity toward each product has similar tendency along solid reduction time. Moreover, when the solid is completely reduced (i.e., up to about 36 min), selectivities reach the same level irrespective of the cycle number.

The global performance for each cycle (i.e., after reduction plus oxidation steps), is clearly identified from Fig. 6. This figure represents the relative value of hydrogen storage density (H_2SD) obtained after each redox cycle, expressed as the ratio of the actual volume of hydrogen released to the theoretical stoichiometric maximum expected for magnetite when reoxidized by steam (r.13) (i.e., 419 N mL g^{-1}). It is classified by cycle number and reduction temperature tested [16].

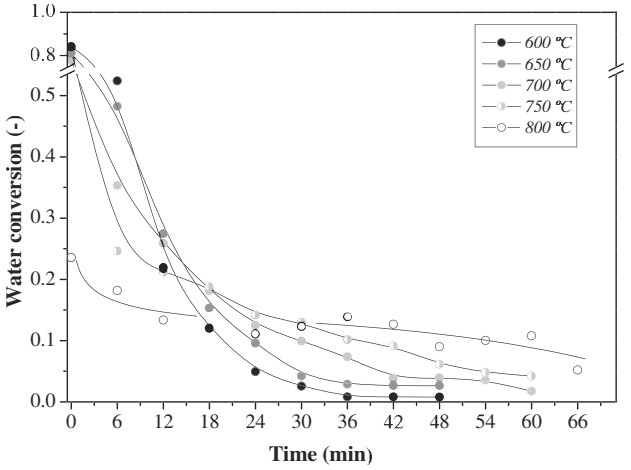

Fig. 4. Temporal evolution of water conversion in the oxidation step at 500 °C as a function of the temperature in the previous reduction step.

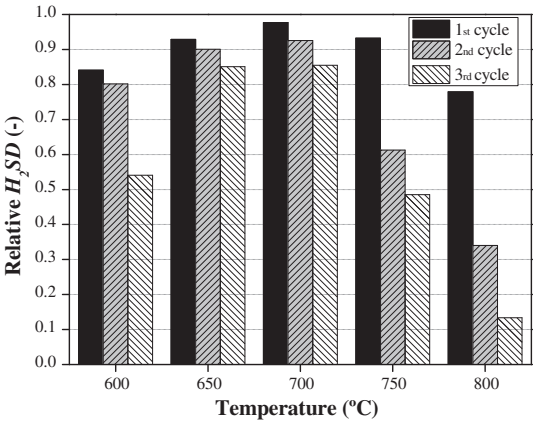

Fig. 6. Hydrogen storage density (H_2SD) relative to the theoretical one for hematite, as a function of cycle number and reduction temperature.

Optimal hydrogen generation was obtained for reduction steps performed at 700 °C. Even though metallic iron shows some wear degree, as it could be expected in view of the behavior of reduction step (Fig. 5), hydrogen release after the third cycle is up to 85% of H_2SD maximum value (to magnetite). In experiments performed with reduction temperatures below 700 °C, hydrogen storage density is lower. This effect is intensified along the cycles (from the first to the third cycle), and it might be associated with coke accumulation over the solid bed surface, which affects solid reactivity by fouling of active sites. In experiments with reduction temperatures above 700 °C, thermal sintering is an important factor of iron exhaustion also leading to lower values of relative hydrogen storage density. This issue is intensified in second and third cycle.

3.6. Carbonaceous depositions

Coke deposited over the solid bed during reduction step with methanol does not react with steam during the oxidation step at 500 °C. Iron oxides (Fe_xO_y) or Fe exert a role as promoters of methanol decomposition, which would produce carbonaceous deposition (r.3) at mild temperatures [6]. At the same time, iron oxides allow CO disproportionation (r.12) at temperatures around 600 °C. As result, carbon filaments are formed [31]. Filamentous depositions are unstable at experimental temperatures (~600 °C), and tend to turn into graphitized structures [6]. When the oxidation step is carried out, the presence of water besides the release of hydrogen (r.13), can promote structured or graphitized growing of coke by adsorption and diffusion effect over iron metallic particles. In this sense, Nasibulin et al. [32] have demonstrated that H_2O and CO_2, fed to the reactor or formed upstream on the bed, can play an important role downstream in the single-walled carbon nanotubes (CNTs) growth. This hypothesis is also supported by the work of Hata et al. [33], who have recently demonstrated the importance of water vapor in providing conditions for efficient growth of CNT forests from methane.

In order to verify the structure of carbon deposits, several essays were performed using SEM and TEM. Fig. 7a shows SEM analysis of a coked sample, taken after the oxidation step of a series of three redox cycles (reductions of triple oxide by methanol at 650 °C and reductions with steam at 500 °C). Depositions have filamentous structure, with space random arrangement and variable dimensions (nanotube diameters from 20 to 50 nm and length between 200 nm and close to 1 μm). Inner structure was identified by TEM technique (Fig. 7b and c). The picture on the left, (Fig. 7b) shows one of the filaments as a hollow structure with straight walls. In order to explain the formation of these tubes, the right picture (Fig. 7c) indicates that the generation of these nanotubes is promoted from metallic particles (Fe) found in the tip of the structure.

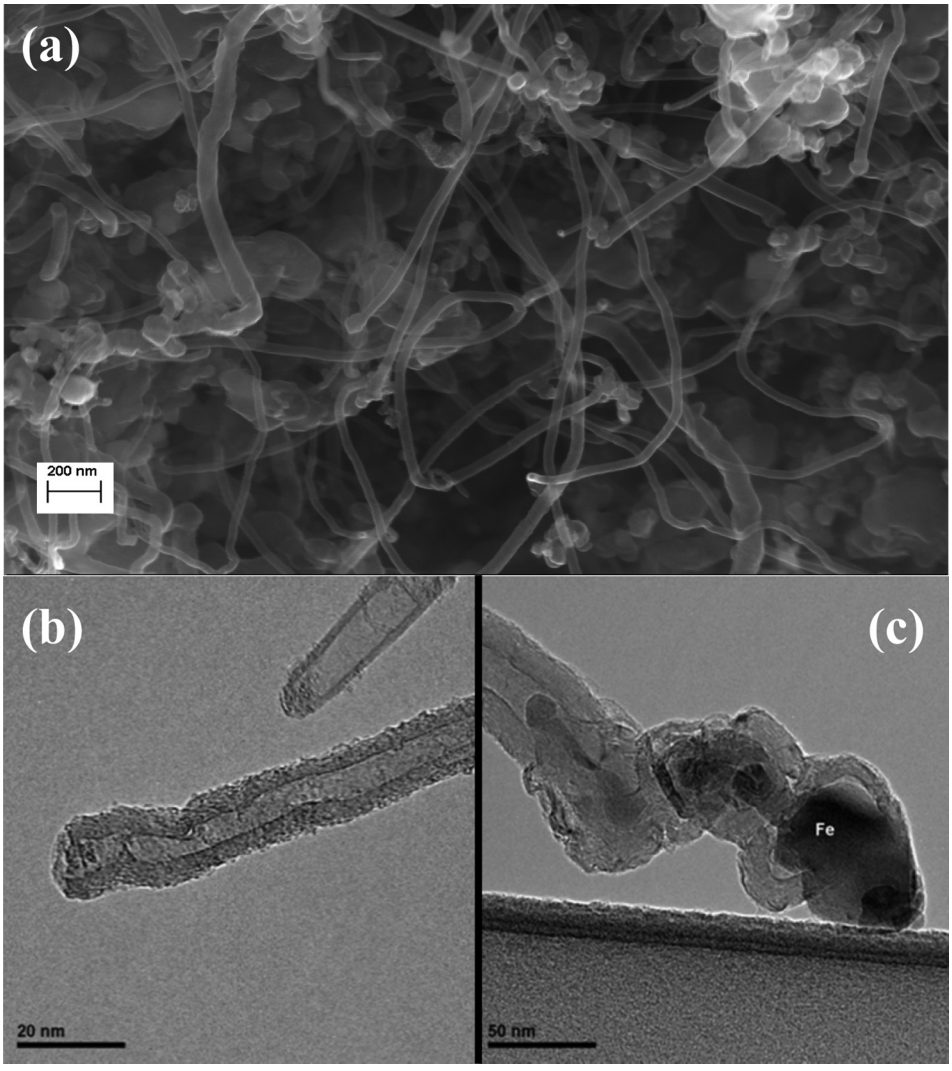

Fig. 7. (a) SEM image of coke and (b, c) TEM images of carbon filaments after three redox cycles (reduction steps at 650 °C, oxidation steps at 500 °C).

Since the accumulated coke is not removed by the oxidation steps with steam, an efficient removal method for carbonaceous deposits is needed in order to allow continuous application of the SIP process. In this sense, combustion experiments were carried out with diluted air in a thermobalance. Results (not shown) indicate that coke can be removed by combustion in air from 450 to 650 °C. Thus, periodic inclusion of a decoking stage in the SIP process would allow carbon removal in a separate stream apart from that where hydrogen is obtained.

On this way, the steam–iron process with methanol as reducing agent, and unlike simple catalytic decomposition, allows obtaining a hydrogen stream free of CO or CO_2. These species could be separated as a stream coming from reduction step (mainly CO mixed with H_2), and a coke combustion exhaust stream (CO_x).

4. Conclusions

The use of doped iron oxides supposes an alternative to simultaneous production and purification of hydrogen using redox processes. This system could be used in exploitation of bio-oils from agro-wood wastes. Iron oxides act as catalysts and decompose methanol completely into CO and H_2. Although coke is formed over solid bed during the reduction step, this deposition is constituted by filaments with high graphitization level. This coke adopts an inert role during oxidation steps with steam at 500 °C. On this way, carbon is preserved and hydrogen released keeps its purity with CO_x species below 50 ppm. Optimum temperature scheme for the process was found to be 700 °C for reductions and subsequent oxidations at 500 °C. These allow a minimum solid exhaustion and high hydrogen release (up to 85% of the theoretical maximum) along cycles. Further investigations should be focused on strategies to increase the hydrogen storage capacity from the first cycle, approaching to the stoichiometric theoretical value, and therefore improving the stability of the process along cycles.

Acknowledgments

Financial support for this research has been provided by the Spanish *Ministerio de Ciencia e Innovación* (MICINN), through project ENE2010-16789. J. Plou also thanks the same institution for the grant BES-2011-045092. Financial aid for the maintenance of the consolidated research group CREG has been provided by the *Fondo Social Europeo* (FSE) through the *Gobierno de Aragón* (Aragón, Spain).

References

[1] M. Bertero, F. de la Puente, U. Sedran, Fuel 95 (2012) 263–271.
[2] K. Sipilä, E. Kuoppala, L. Fagernäs, A. Oasmaa, Biomass Bioenergy 14 (1998) 103–113.
[3] S. Fukase, T. Suzuka, Can. J. Chem. Eng. 72 (1994) 272–278.
[4] F. Gong, T. Ye, L. Yuan, T. Kan, Y. Torimoto, M. Yamamoto, Q. Li, Green Chem. 11 (2009) 2001–2012.
[5] M.F. Bleeker, H.J. Veringa, S.R.A. Kersten, Ind. Eng. Chem. Res. 49 (2010) 53–64.
[6] W.L. Holstein, Ind. Eng. Chem. Res. 33 (1994) 1363–1372.
[7] V. Hacker, R. Frankhauser, G. Falsechini, H. Fuchs, K. Friedrich, M. Muhr, K. Koldesch, J. Power Sources 86 (2000) 531–535.
[8] S.J. Gasior, A. Forney, J. Field, D. Bienstock, H. Benson, Report of Investigations 5911, United States Department of Interior, Bureau of Mines, 1961.
[9] M.F. Bleeker, S.R.A. Kersten, H.J. Veringa, Catal. Today 127 (2007) 278–290.
[10] J.A. Peña, E. Lorente, E. Romero, J. Herguido, Catal. Today 116 (2006) 439–444.
[11] E. Lorente, J.A. Peña, J. Herguido, Int. J. Hydrogen Energy 33 (2008) 615–626.
[12] E. Lorente, Q. Cai, J.A. Peña, J. Herguido, N.P. Brandon, Int. J. Hydrogen Energy 34 (2009) 5554–5562.
[13] C. Sanz, J. Plou, P. Durán, J.A. Herguido, J.A. Peña, Hydrogen from synthetic biogas by dry reforming and steam–iron; reaction mechanism. I. International Congress of Chemical Engineering (ICCE 2012), Conference Book of Abstracts, T8-016, Sevilla (Spain), ISBN 988-84-695-3536-3.
[14] J. Berenguer, P. Duran, E. Romero, J. Herguido, J.A. Peña, Hydrogen production from biogas using redox oxides in a fixed bed reactor, World Hydrogen Energy Conference WHEC – Toronto, 2012, p. A97.
[15] J. Plou, P. Duran, E. Romero, J. Herguido, J.A. Peña, Modified metal oxides for energy and hydrogen production from biogas, STA thermogravimetric study of the reduction step, in: 20th International Congress of Chemical and Process Engineering CHISA – Prague 2012, ISBN 978-80-905035-1-9.
[16] E. Lorente, J.A. Peña, J. Herguido, Int. J. Hydrogen Energy 36 (2011) 7043–7050.
[17] E. Lorente, J.A. Peña, J. Herguido, J. Power Sources 192 (2009) 224–229.
[18] S. Takenaka, K. Nomura, N. Hanaizumi, K. Otsuka, Appl. Catal. A: Gen. 282 (2005) 333–341.
[19] K. Otsuka, C. Yamada, T. Kaburagi, S. Takenaka, Int. J. Hydrogen Energy 28 (2003) 335–342.
[20] J.C. Ryu, D.H. Lee, K.S. Kang, C.S. Park, J.W. Kim, Y.H. Kim, J. Ind. Eng. Chem. 14 (2008) 252–260.
[21] S. Damyanova, B. Pawelec, K. Arishtirova, M.V. Martínez Huerta, J.L.G. Fierro, Appl. Catal. A: Gen. 337 (2008) 86–96.
[22] A. Palacios, L. Martinez, E. Romero, P. Duran, J. Herguido, J.A. Peña, Effect of impurities of the solid on the subsequent hydrogen release in steam–iron process, in: D. Stolten, T.E. Grube (Eds.), 18th World Hydrogen Energy Conference – Essen (Germany), Forschungszentrum Jülich GmbH, Zentralbibliothek, Verlag, Essen, 2010, p. 379.
[23] P. Duran, E. Romero, J. Herguido, J.A. Peña, Separation and storage of hydrogen by redox process using modified iron oxides in a fixed bed reactor. I. Simposium Ibérico de Hidrógeno, Pilas de Combustible y Baterías Avanzadas, HYCELTEC – Bilbao (Spain), 2008, ISBN 978-84-9860-101-5.
[24] J. Kirchnerova, M. Alifanti, B. Delmon, Appl. Catal. A: Gen. 231 (2002) 65–80.
[25] M.P. Kapoor, A. Raj, Y. Matsumura, Micropor. Mesopor. Mater. 44–45 (2001) 565–572.
[26] S.D. Jackson, D.S. Anderson, G.J. Kelly, T. Lear, D. Lennon, S.R. Watson, Top. Catal. 22 (2003) 173–182.
[27] E. Manova, T. Tsoncheva, C.L. Estournès, D. Paneva, K. Tenchev, I. Mitov, L. Petrov, Appl. Catal. A: Gen. 300 (2006) 170–180.
[28] E. Lorente, J.A. Peña, J. Herguido, Int. J. Hydrogen Energy 36 (2011) 13425–13434.
[29] W.K. Jozwiak, E. Kaczmarek, T. Maniecki, W. Ignaczak, W. Maniukiewicz, Appl. Catal. A: Gen. 326 (2007) 17–27.
[30] J. Plou, P. Duran, J. Herguido, J.A. Peña, Int. J. Hydrogen Energy 37 (2012) 6995–7004.
[31] A.S. Anisimov, A.G. Nasibulin, H. Jiang, P. Launois, J. Cambedouzou, S.D. Shandakov, E.I. Kaupinnen, Carbon 48 (2009) 380–388.
[32] A.G. Nasibulin, D.P. Brown, P. Queipo, D. Gonzalez, H. Jiang, E.I. Kauppinen, Chem. Phys. Lett. 417 (2006) 179–184.
[33] K. Hata, D.N. Futaba, K. Minuzo, T. Namai, M. Yumura, S. Ijima, Science 306 (2004) 1362–1364.